EFDA–JET–CP(12)02/08

A. Järvinen, M. Groth, D. Moulton, J. Strachan, S. Wiesen, P. Belo, M. Beurskens, G. Corrigan, T. Eich, C. Giroud, E. Havlickova, S. Jachmich, M. Lehnen, J. Lönnroth, D. Tskhakay and JET EFDA contributors

Simulations of Tungsten Transport in the Edge of JET ELMy H-Mode Plasmas

Simulations of Tungsten Transport in the Edge of JET ELMy H-Mode Plasmas

A. Järvinen[1], M. Groth[1], D. Moulton[2], J. Strachan[3], S. Wiesen[4], P. Belo[5], M. Beurskens[6], G. Corrigan[6], T. Eich[7], C. Giroud[6], E. Havlickova[6], S. Jachmich[8], M. Lehnen[4], J. Lönnroth[1], D. Tskhakay[9] and JET EFDA contributors*

JET-EFDA, Culham Science Centre, OX14 3DB, Abingdon, UK

[1]Aalto University, Association EURATOM-Tekes, P.O.Box 14100, FI-00076, Finland
[2]EURATOM/CEA Fusion Association, Cadarache FR IRFM, F-13108, St-Paul-lez-Durance, France
[3]PPPL Princeton University, Princeton, NJ 08543, USA
[4]Forschungszentrum Jülich GmbH, EURATOM-Assoziation, TEC, D-52425 Jülich, Germany
[5]EURATOM/IST Fusion Association, IPFN, Av. Rovisco Pais 1049-001 Lisbon, Portugal
[6]EURATOM/CCFE Fusion Association, Culham Science Centre, Abingdon, Oxon, OX14 3DB, UK
[7]Max-Planck-Institut für Plasmaphysik, EURATOM-Assoziation, D-85748 Garching, Germany
[8]Ecole Royale Militaire, EURATOM-Association, Brussels, Belgium
[9]University of Innsbruck, Association EURATOM-ÖAW, A-6020 Innsbruck, Austria
** See annex of F. Romanelli et al, "Overview of JET Results", (23rd IAEA Fusion Energy Conference, Daejon, Republic of Korea (2010)).*

Preprint of Paper to be submitted for publication in Proceedings of the
20th International Conference on Plasma Surface Interactions , Eurogress, Aachen, Germany
21st May 2012 - 25th May 2012

ABSTRACT

Tungsten contamination can significantly impact the performance of future fusion reactors via fuel dilution and radiation in the plasma centre. Therefore, understanding tungsten sputtering and divertor retention is essential for optimising the core performance in tokamaks operating with tungsten. This study investigates these issues numerically in JET high-triangularity, type-I ELMy H-mode plasmas with the Monte-Carlo code DIVIMP used on background plasmas dynamically evolved with the multi-fluid code EDGE2D/EIRENE. During the ELM, the simulations show target temperatures in excess of a few 100eV, causing two orders of magnitude increase in the tungsten core contamination rate. During the ELM recovery, target densities of five times the pre-ELM values are obtained at the low field side, which strongly enhance divertor retention via increased friction with the main ions. Therefore, the core contamination is determined here dominantly by the intra-ELM divertor plasma characteristics.

1. INTRODUCTION

Tungsten Plasma-Facing Components (PFCs) are foreseen in the divertor of ITER during the activated operational phase due to low fuel retention in the bulk material and absence of co-deposition [1]. While tungsten is resilient against physical sputtering by deuterium in semi-detached plasma conditions, Edge Localised Modes (ELMs) and plasma impurities may lead to considerable tungsten erosion and contamination in the plasma centre, therefore reducing the reactor performance. Despite the detrimental effects of ELMs for the PFCs, type-I ELMy H-mode is considered as one of the leading candidate high-performance operational regimes in the future fusion reactors. Therefore, it is essential to understand tungsten erosion and transport processes in ELMy H-mode plasmas to optimise the reactor performance in tokamaks operating with tungsten PFCs. To address these issues, an ITER-Like Wall (ILW) was installed in JET with tungsten divertor PFCs and beryllium main chamber limiters [2]. This study numerically investigates tungsten divertor sputtering and scrape-off layer (SOL) transport in one of JET's primary operational scenarios: a high-triangularity, type-I ELMy H-mode plasmas established and characterised in JET's previous carbon wall configuration [3, 4]. This is accomplished by using the quasi-kinetic Monte-Carlo code DIVIMP [5] on background plasmas dynamically evolved with the multi-fluid code EDGE2D/EIRENE [6, 7, 8].

2. ELM SIMULATIONS

A set of high-performance, deuterium-fuelled and nitrogen-seeded reference plasmas in JET's former carbon (CFC) wall configuration were previously established [3, 4]. The simulations presented here are based on one of the reference plasmas: JET Pulse No: 76666, 2.7T/2.5MA, $P_{in} \sim 16$MW, $n_e \sim 0.8 n_{GW}$, high triangularity $d \sim 0.4$, $q_{95} \sim 3.5$, $f_{ELM} \sim 20 - 25$Hz. The pedestal electron temperatures of about 800eV and densities of about 6e19 m^{-3}, measured for JET Pulse No: 76666 [3], give pedestal neoclassical electron collisionalities [9], $n^*_{e,ped}$, of about 0.35 and the pedestal stored energy, W_{ped}, of about 1.8MJ. The effective charge-state of the plasma was measured around $Z_{eff} \sim 1.6 - 1.9$ [3].

In this series of discharges, JET Pulse No: 76666 represents the lowest density reference plasma without nitrogen seeding. The mean ELM size in this discharge was 200–300kJ, interpreted from the temporal evolution of the plasma diamagnetic energy.

This discharge is simulated with EDGE2D/EIRENE. First, a steady state, pre-ELM solution is obtained, and, based on that, ELMs are simulated *ad hoc* by enhancing the cross-field diffusion for a short duration uniformly around the Outer Mid-Plane (OMP) to transfer plasma from the pedestal to the SOL plasma, similar as in ref [10]. The pre-ELM simulation is based on results obtained in [11] for the same discharge. Here, a radially wider simulation grid was used than in ref [11], to span the ELM affected area in the core plasma (Fig.1a). Associated to this, and to improved experimental OMP profiles, the cross-field thermal conduction was slightly increased in the core and within the Edge Transport Barrier (ETB, Fig. 1b), and the conduction ETB width was slightly decreased to enhance the match of the OMP electron density, n_e, and temperature, T_e, profiles with the deconvolved High-Resolution Thomson Scattering (HRTS) measurements. The HRTS profiles are obtained from JET Pulse No: 79498, which is a companion discharge to JET Pulse No: 76666 with twice as much spatial resolution in the pedestal region [12]. To simplify the simulations, zero cross-field convection ($v_{pinch} = 0$) was assumed. In addition, heat-flux limiters of 1.5 were used in this study, whereas they were not used in ref [11]. The HRTS profiles are shifted 1.05 cm outwards from the locations suggested by the magnetic equilibrium reconstruction (EFIT) by assuming OMP separatrix T_e of 160 +/- 40 eV, calculated with the standard 2-point model [13]. The pre-ELM EDGE2D/EIRENE (E2D) simulations are matched within a factor of 1.5 to OMP values of n_e and T_e from HRTS, as well as to the outer target LP and IRTV measurements of T_e, ion saturation current, j_{sat}, outer target power, P_{OT}, and maximum outer target heat flux density, $q_{OT,\,max}$: $T_e^{LP} \sim 40$eV, $T_e^{E2D} \sim 50$eV; $j_{sat}^{LP} \sim 1$MA/m^2, $j_{sat}^{E2D} \sim 1.5$MA/m^2; $P_{OT}^{IRTV} \sim 4$MW, $P_{OT}^{E2D} \sim 4.5$ MW; $q_{OT,\,max}^{IRTV} \sim 17.5$MW, $q_{OT,\,max}^{E2D} \sim 25$MW.

ELMs are simulated by multiplying the cross-field diffusion coefficients uniformly for a short duration on a specific section on the grid (ELM model area) as illustrated in the Fig. 1. Two ELM durations are considered: 0.2 and 1ms. The 0.2ms corresponds to the average observed ELM duration interpreted from the length of the ELM related magnetic fluctuation phase with the previous CFC first wall [14]. The ELMs in comparable plasmas seem to be much longer with the ILW [15]. The ELM model is adjusted to match the total ELM magnitude and the convective-conductive ELM losses [9] ratio within a factor of two (table 1). The experimental estimate for the latter is obtained from [9], taking into account the $n^*_{e,\,ped} \sim 0.35$ in JET Pulse No: 76666. Accordingly, the convective losses are assumed to cause approximately 4–8% loss of W_{ped} (~ 110 +/-30 kJ), and the conductive losses are assumed to cause a loss of 3–10% of W_{ped} (~ 120 +/-60 kJ). The ELM losses in EDGE2D/EIRENE simulations are calculated using the equation (1) in [9].

3. TUNGSTEN CONTAMINATION STUDIES FOR JET TYPE-I ELMY H-MODE PLASMAS

3.1. DIVIMP SIMULATION DETAILS

Tungsten erosion and transport are simulated with DIVIMP using the obtained EDGE2D/EIRENE solutions as time evolving series of background plasmas. Erosion of tungsten and its transport across the separatrix to the core, giving the core leakage fraction, are calculated with DIVIMP on a steady-state fashion for the individual time slices in the series. The tungsten particles entering the core are not followed further due to insufficient core plasma model in DIVIMP. Tungsten core contamination rate is interpreted from the DIVIMP calculations by multiplying the tungsten erosion rate during a specific time slice with an average tungsten core leakage fraction within the following time slices. The length of the averaging procedure is given by the average time that it takes a particle to cross the separatrix within that specific time slice for which the core contamination rate is interpreted. The time averaging lengths in this study appeared to be approximately 200–500μs during the intra-ELM phase, and approximately 500–1500μs during the ELM recovery phase. The interval between subsequent time slices is 100μs within -0.1–1.9ms after the ELM onset, 1 ms within the 1.9–10.9ms after the ELM onset, and 10 ms within 10.9–40.9ms after the ELM onset. The ELM frequency in JET Pulse No: 76666 was 20–25Hz; therefore, the ELM recovery phase was not calculated beyond 40 ms after the ELM onset.

Erosion of tungsten due to background deuterium and 1% carbon 4+ as a proxy for light, medium-charged impurities are taken into account. The sputtering yields for deuterium and carbon impacts are given by the Eckstein 2007 and 1996 data [16, 17], respectively. Normal incidence yields are used for the sputtering calculations. Atomic rates for tungsten are obtained from ADAS 1997 database [18]. Tungsten is assumed to re-deposit promptly during its first gyro orbit if it ionizes within its Larmor radius from a solid structure. Tungsten self-sputtering is not included in the series of the main simulations due to interpretation issues related to the steady-state runs with DIVIMP: here, self-sputtering will be studied in an additional set of simulations.

The transport of tungsten neutrals is calculated by the Monte-Carlo neutral code EIRENE [7]. After ionization, the tungsten ions are transported on a 2-D grid assuming parallel-**B** forces due to the impurity pressure gradient, background ion friction, electric field, and thermal forces due to electrons and ions [19] and cross-field diffusion with a diffusion coefficient of 1 m^2/s. In [20] it has been demonstrated that the fluid forces do not take into account the kinetic velocity dependence of the thermal and friction forces. The effect of these kinetic corrections will be investigated in an additional set of simulations.

3.2. TUNGSTEN TRANSPORT SIMULATION RESULTS

The core tungsten contamination calculated by DIVIMP is strongly dominated by the intra-ELM phase (Fig.2). During the first few 100μs after the ELM onset, the simulated ELMs lead to sheath-limited (SOL electron collisionality, $\nu_e \sim 1$) SOL conditions with target temperatures in excess of

a few 100eV, and target densities of approximately a factor of five lower than the pre-ELM values (Fig. 2). ν_e stands for the ratio of the electron collisional mean free path to the half of the separatrix parallel-**B** connection length, $L_{\sqcap}$. The sheath-limited conditions are followed by a high recycling phase approximately 500 – 1500 μs after the ELM onset. During the high recycling phase, the target densities are approximately a factor of five higher compared to the pre-ELM values and the target temperatures drop down to values ranging from below 1 to 25 eV. The SOL density remains elevated for several milliseconds after the ELM onset. This dynamics leads to significant increase of tungsten sputtering and divertor leakage during the sheath-limited phase, followed by suppression of both during the high-recycling ELM recovery phase (Fig. 2). The average initial velocity of the sputtered atoms, which is calculated according to the kinetic energy of the impinging particles [21], is increased by 15 % during the sheath-limited phase compared to the pre-ELM phase. Friction of tungsten with main ions scales as $n/T_i^{3/2}$ [19, 22], where T_i stands for the temperature of the main ions. Therefore, as the plasma collisionality, $n^* \mu\ n/T^2$, during the sheath-limited intra-ELM phase drops significantly, the collisional coupling of the impurity ions to the background deuterium flow is reduced. Accordingly, the intra-ELM phase leads to (a) a significant release of tungsten and a considerable increase of the initial velocity of the sputtered atoms, and (b) to notable decrease in the background friction. Consequently, the intra-ELM phase leads to significant increase of the tungsten core penetration rate and thus dominates the total core contamination. Similarly in ref [23], in DIVIMP simulations on background plasmas dynamically evolved with the integrated code suite JINTRAC [24] for a JET low-triangularity ILW reference plasma [25], ELMs were found to increase significantly the tungsten sputtering and core leakage.

The DIVIMP here predicts approximately 1.5e17 tungsten particles entering the core per an ELM cycle (Fig.2). With the ELM frequency of 20 Hz, this indicates an average tungsten core contamination rate of 3e18 W/s. Assuming a core confinement time of 60 ms, a core density of 7e19 m^{-3} and a core plasma volume of 100m^3, this estimate results in a tungsten core concentration of approximately a few 10^{-5}. The assumed confinement time is obtained using the equation (14) in [26] with values $L_{//}/c_{s,W} \sim 3$ ms, $f_{ELM} \sim 20$Hz and $D_{SOL} \sim 1$ m^2/s. The tungsten sound speed, $c_{s,W}$, has been calculated assuming an ensemble temperature equal to one third of the pedestal temperature: ~ 250eV. Assuming flat temperature profiles in the core of approximately 2keV, this gives an estimated core tungsten radiative power of 1–2MW (equation (4.25.1) in [27]). The reader should note that these calculations are, however, approximative, used only for giving a context for the obtained DIVIMP calculations. Therefore, further studies are required to address the tungsten core confinement issue in more detail.

Approximately 50 % of the core tungsten contamination in the simulations originated from sputtering due to deuterium. Tungsten self-sputtering is neglected here. Accordingly, the intra-ELM deuterium sputtering is anticipated to cause tungsten contamination comparable to the values caused by sputtering due light impurities. Therefore, as the sputtering and divertor retention depend strongly on the plasma temperature, SOL plasma seeding is anticipated to decrease the core tungsten

contamination by lowering the divertor plasma temperatures, although the seeding increases the light impurity concentration in the divertor plasma.

An additional set of simulations for the 1 ms ELM case suggests that considerable tungsten self-sputtering is anticipated for a few 100 μs during the intra-ELM phase. Therefore, the ELM-induced tungsten erosion may be significantly enhanced by self-sputtering. This process is, however, very sensitive to the kinetic evolution of the sheath during the ELM onset, and this is not included in the EDGE2D/EIRENE simulations executed here. Therefore, the dynamics of the sheath potential, which largely determines the impact energy of the plasma particles, are not followed and will be addressed in subsequent studies.

A sensitivity study for the 1 ms ELM case with the drift-kinetic impurity forces, as give in [20], demonstrates a factor of two higher divertor retention during the intra-ELM phase compared to the fluid force approach. During the far ELM recovery phase (> 20ms after the ELM onset), the retention is approximately a factor of four to five higher. Therefore, the tungsten contamination values obtained with the fluid force approach here can be overestimated approximately by a factor of two, as most of the contamination occurs during the intra-ELM phase. The obtained qualitative dynamics do not, however, differ between the approaches.

CONCLUSION

Tungsten erosion and transport are simulated for one of the JET type-I ELMy H-mode ILW reference plasmas, obtained with the CFC wall, by using DIVIMP on background plasmas dynamically evolved with EDGE2D/EIRENE. The simulated ELMs lead to a cycle of sheath-limited plasma conditions with target temperatures exceeding a few 100 eV during the first few 100 μs after the ELM onset, followed by high-recycling conditions with target temperatures of about 1 – 25 eV approximately 500 – 1500 μs after the ELM onset. The SOL density remains elevated several milliseconds after the ELM onset. This dynamics leads to significantly increased tungsten sputtering and core contamination during the sheath-limited intra-ELM phase, via increased sputtered velocity and suppressed background ion friction. The high recycling conditions during the ELM recovery phase lead to suppression of tungsten sputtering and core leakage, via lowered target temperatures and increased divertor collisionalities. Therefore, according to the simulations in this study, the tungsten core contamination of ELMy H-mode plasmas is strongly determined by the ELM divertor plasma characteristics in the scrape-off layer. On the other hand, ELMs are also considered as the dominant process of the reducing the core tungsten contamination, hence, core-edge integrated simulations are necessary to characterise the combined effect. The simulations show approximately 50 % of the core tungsten contamination originating from sputtering due to deuterium, when self-sputtering is neglected. Accordingly, increasing the light impurity concentration in the divertor plasma is not anticipated to increase the tungsten impurity source significant, while the core tungsten contamination is anticipated to be decreased due to lowered divertor temperatures and increased collisionalities.

ACKNOWLEDGEMENTS

This work, supported by the European Communities under the contract of association between EURATOM/TEKES was carried out within the framework of the European Fusion Development Agreement. The views and opinions expressed herein do not necessarily reflect those of the European Commission. The work was also partly funded by the Academy of Finland under the grant number 13253222.

REFERENCES

[1]. R. A. Pitts, et al. Physica Scripta **T138** (2009) 014001.
[2]. G. F. Matthews, et al., Physica Scripta **T145** (2011) 014001.
[3]. C. Giroud, et al., Proc. 23rd IAEA Fusion Energy Conf. EXC/P3-02 (2010).
[4]. G. Maddison, et al., Nuclear Fusion Letters **51** (2011) 042001
[5]. P. C. Stangeby, J. D. Elder, Nuclear Fusion **35** (1995) 1391.
[6]. R. Simonini, et al., Contrib. Plasma Physics **34** (1994) 368.
[7]. D. Reiter, Journal of Nuclear Materials **196 – 198** (1992) 241.
[8]. S. Wiesen, EDGE2D/EIRENE code interface report, JET ITC-Report, http://www.eirene.de/e2deir_report_30jun06.pdf, (2006).
[9]. M. N. A. Beurskens, et al. Nuclear Fusion **49** (2009) 125006.
[10]. A. Kallenbach, et al., Plasma Physics and Controlled Fusion **46** (2004) 431 – 446.
[11]. D. Moulton, et al., Journal of Nuclear Materials **509 – 512** (2011) 415.
[12]. M. N. A. Beurskens, et al., Physics of Plasmas **18** (2011) 056120
[13]. P. C. Stangeby, The Plasma Boundary of Magnetic Fusion Devices, IoP Publishing Ltd 2000, ISBN 0-7503-0559-2.
[14]. A. Loarte, et al., Plasma Physics and Controlled Fusion **45** (2003) 1549 – 69.
[15]. G. F. Matthews, et al., These proceedings.
[16]. W. Eckstein, Sputtering by Particle Bombardment, Springer-Verlag Berlin Heidelberg, (2007), ISBN: 987-3-540-44500-5.
[17]. W. Eckstein, Journal of Nuclear Materials **248** (1997) 1 – 8.
[18]. A. Thoma, et al., Plasma Physics and Controlled Fusion **39** (1997) 1487 – 99.
[19]. J. Neuhauser, et al., Nuclear Fusion **24** (1984) 39 – 47.
[20]. D. Reiser, D. Reiter, M. Z. Tokar, Nuclear Fusion **38** (1998) 165 – 177.
[21]. A. Järvinen, et al., Physica Scripta **T145** (2011) 014013.
[22]. L. Spitzer, Jr., Physics of Fully Ionized Gases, 2nd ed., Interscience Publisher, New York (1962), ISBN 9780486449821
[23]. A. Järvinen, et al., Proc. of 38th EPS conf. on Plasma Physics (2011) P2.067.
[24]. S. Wiesen, et al., JINTRAC-JET modelling suite JET ITC-Report (2008), http://www.eirene.de/JINTRAC_Report_2008.pdf
[25]. S. Wiesen, et al., Plasma Physics and Controlled Fusion **53** (2011) 124039.

[26]. R. Dux, et al., Nuclear Fusion **51** (2011) 053002.

[27]. J. Wesson, Tokamaks, 3rd edition, Oxford University Press (2004), ISBN 0 19 8509227

	t_{ELM} [ms]	$M_{D^\wedge}$	$M\chi_{i^\wedge}$	$M\chi_{e^\wedge}$	W_{ELM} [kJ]	$W_{\mathrm{Conv.}}$ [kJ]	$W_{\mathrm{Cond.}}$ [kJ]
Sim. Slow ELM	1	300	75	25	213	98	132
Sim. Fast ELM	0.2	3000	1500	500	175	67	123
Exp. values					200 - 300	110 +/- 30	120 +/- 60

Table 1: The simulated long (1 ms) and short (0.2 ms) duration ELMs compared to the experimental estimations. t_{ELM} stands for the duration of the ELM, $M_{D^\wedge}$ for the cross-field diffusion coefficient multiplier, $M\chi_{i^\wedge}$ for the ion cross-field conduction multiplier, $M\chi_{e^\wedge}$ for the electron cross-field conduction multiplier and W_{ELM}, $W_{Conv.}$ and $W_{Cond.}$ for the total, convective and conductive ELM losses.

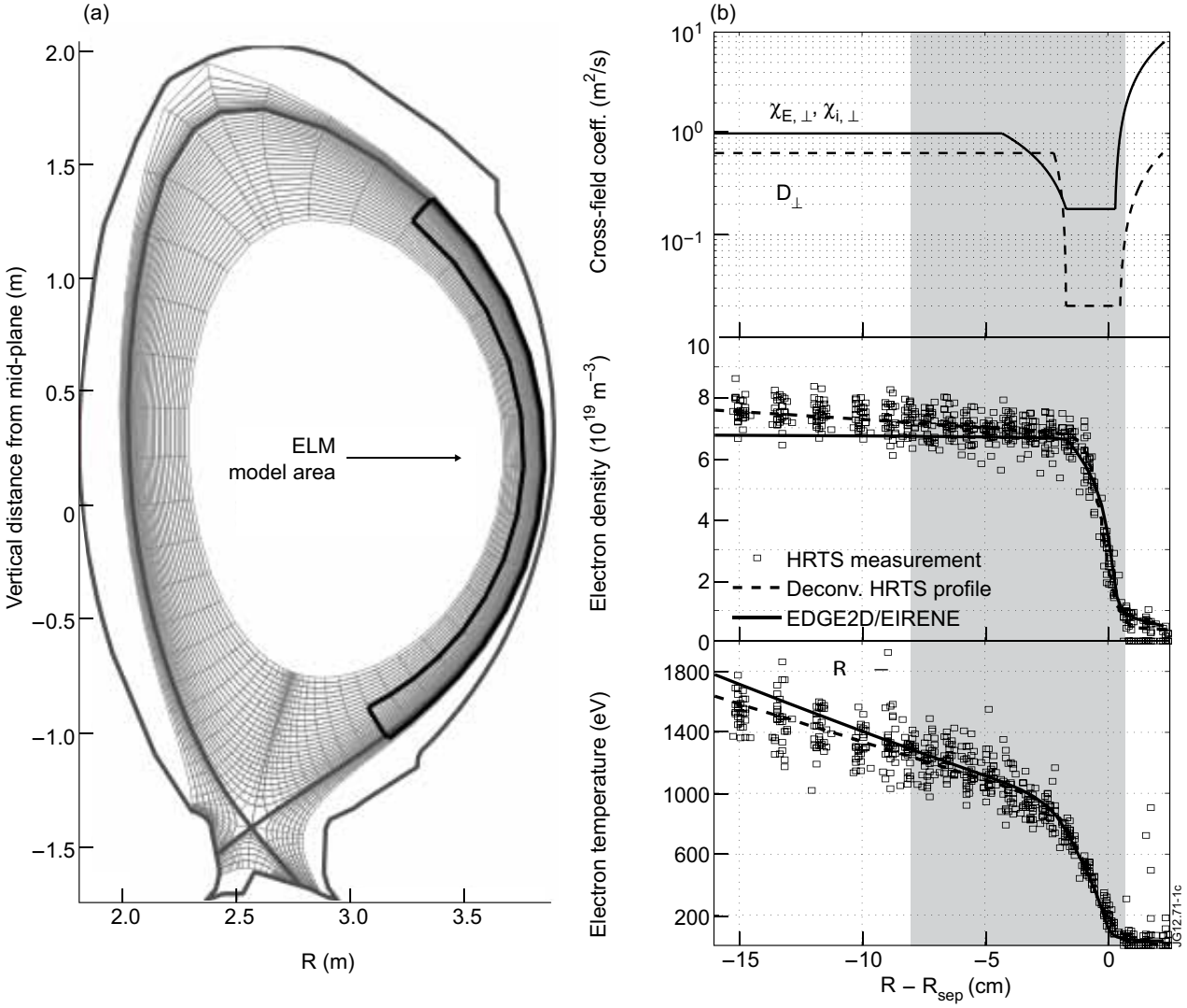

Figure 1: a) EDGE2D/EIRENE and DIVIMP simulation grid used in this study. The separatrix is shown in blue, and the affected area of the ELM model is outlined with the red line. b) The cross-field diffusion coefficients used in the study. The pre-ELM EDGE2D/EIRENE outer mid-plane profiles (black) of electron density, n_e, and temperature, T_e, as well as the deconvolved HRTS profiles from the discharge JPN 79498 (grey). The simulate T_i value is illustrated with the dashed line. The HRTS data is shown with grey squares. The ELM model affects the shadowed area.

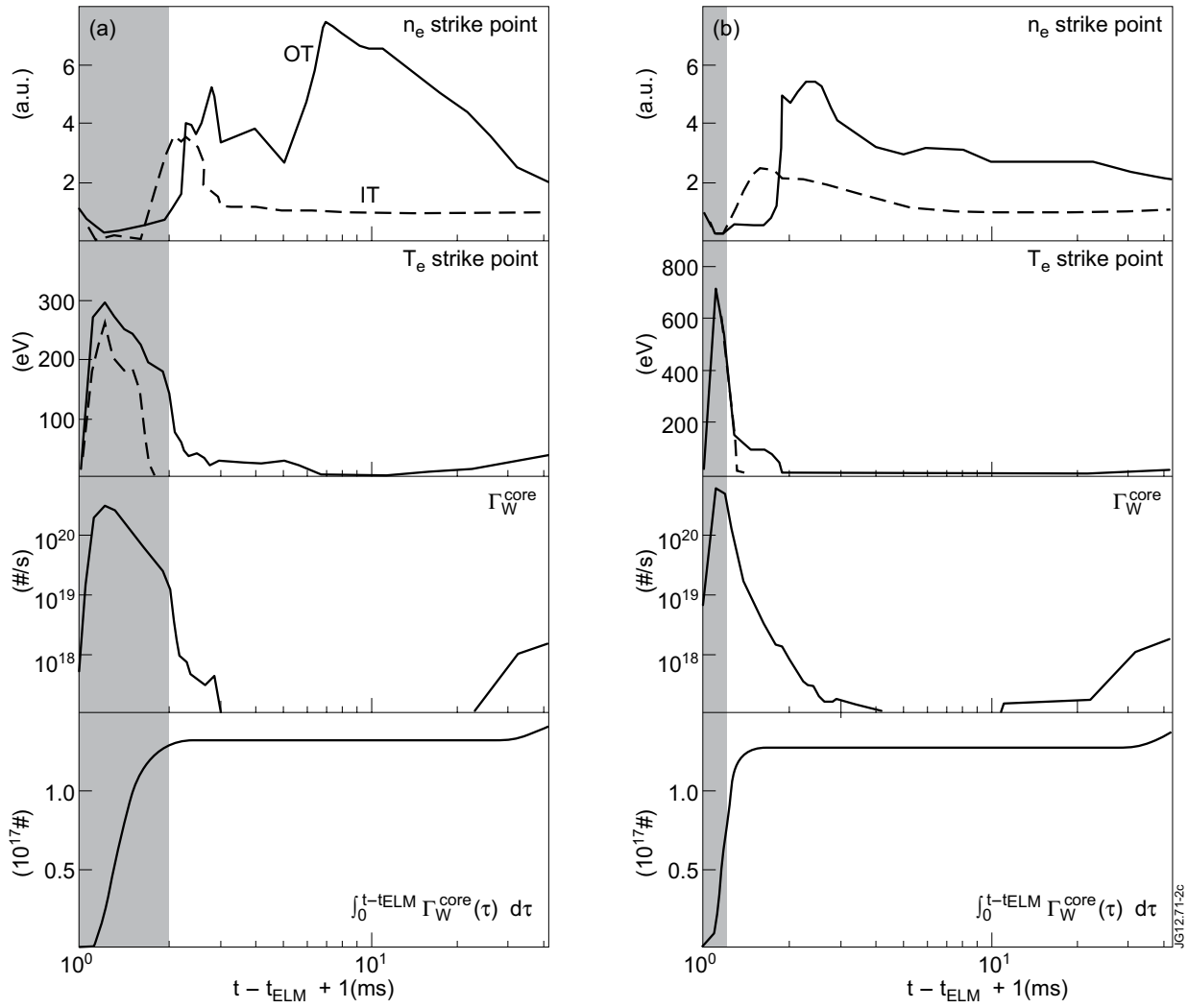

Figure 2: ELM evolution of strike point electron density, n_e, and temperature, T_e, core tungsten contamination rate, $\Gamma_{W,\ core}$, and integrated core tungsten contamination over the ELM cycle for 1 ms (a) and 0.2 ms (b) ELMs. The electron densities are normalized to their pre-ELM values. The inner target (IT) strike point values are plotted with dashed lines, and the outer target (OT) strike point values with solid lines. The shadowed area marker the assumed intra-ELM phase (of enhanced outer mid-plane cross-field diffusion). The reader should note that the logarithmic time axis.